UMYU Scientifica, Vol. 5 NO. 2, June 2026, Pp 312 – 322
https://doi.org/10.56919/usci.2652.029
ISSN: 2955 – 1145 (print); 2955 – 1153 (online)
*A periodical of the Faculty of Natural and Applied Sciences, UMYU, Katsina*

ORIGINAL RESEARCH ARTICLE

# Chalcogen Vacancy Engineering in 1T-$TiS_2$, 1T-$TiSe_2$ and 1T-$TiTe_2$ Monolayers for Enhanced HER Activity: A DFT Study

Shamsuddeen Sani Alhassan*, Mahmud Abdulsalam, Abdullahi Tanimu and Muhammad Ibrahim Bagudo
Department of Physics, Umaru Musa Yar'adua University, P.M.B. 2218, Katsina State, Nigeria

## ABSTRACT
Electrocatalytic water splitting offers a sustainable pathway for green hydrogen production, yet its widespread adoption requires low-cost and earth-abundant alternatives to platinum-group metal catalysts. Herein, we present a systematic density functional theory (DFT) study of chalcogen vacancy engineering on the catalytic performance of 1T-$TiX_2$ (X = S, Se, Te) monolayers in hydrogen evolution reaction (HER). Our calculations reveal that pristine 1T-$TiX_2$ surfaces exhibit poor hydrogen adsorption, with 1T-$TiS_2$ lying on the strong-binding side, while 1T-$TiSe_2$ and 1T-$TiTe_2$ reside on the weak-binding side of the volcano curve, explaining their unfavourable catalytic activity. The introduction of single chalcogen vacancies dramatically shifts all systems toward the volcano apex, with defective 1T-$TiS_2$ achieving a near-thermoneutral Gibbs free energy of hydrogen adsorption ($\Delta G_{H^*}$) of -0.08 eV, thermodynamically comparable to the benchmark Pt (111) value (-0.09 eV). This promising computational result requires experimental validation. Defect formation energies are positive for all systems (3.53 eV, 2.73 eV, and 2.12 eV for S, Se, and Te vacancies, respectively), indicating thermodynamic stability of the vacancy configurations under computational chemical-potential conditions. Electronic structure analysis further demonstrates that vacancy-induced metallization generates prominent states at the Fermi level, thereby enhancing charge-transfer kinetics. Notably, 1T-$TiS_2$ undergoes a semimetallic to metallic transition upon S-vacancy creation, whereas 1T-$TiSe_2$ and 1T-$TiTe_2$ show moderate electronic enhancement. This work establishes chalcogen-vacancy engineering as a universal strategy for activating the 1T-$TiX_2$ basal planes. It identifies defective 1T-$TiS_2$ as the most promising, cost-effective, and non-precious HER catalyst within the 1T-$TiX_2$ family, providing design principles for next-generation sustainable hydrogen production technologies.

## ARTICLE HISTORY
Received February 25, 2026
Accepted June 24, 2026
Published June 26, 2026

## KEYWORDS
Hydrogen evolution reaction; Titanium dichalcogenides; Vacancy engineering; Density functional theory; Electrocatalysis; Green hydrogen.



## INTRODUCTION
The urgent global transition toward sustainable energy systems requires the development of efficient, cost-effective technologies for clean hydrogen production (Staffell et al., 2019). Electrocatalytic water splitting via the hydrogen evolution reaction (HER) is a promising pathway for producing green hydrogen, yet its widespread adoption hinges on replacing scarce and expensive platinum-group metal (PGM) catalysts with earth-abundant alternatives (Zhu et al., 2020; Stamenkovic et al., 2017). Among the leading candidates, layered transition-metal dichalcogenides (TMDs) have attracted significant attention due to their unique properties, including tunable electronic structures, high surface-to-volume ratios, and compositional versatility (Chhowalla et al., 2015; Sukanya et al., 2022; Alhassan et al., 2025).

TMDs with the general formula $MX_2$ (M = transition metal, X = chalcogens either S, Se, or Te) exhibit diverse polytypes (1T, 2H, 3R), with the metallic 1T-phase offering superior intrinsic conductivity which is a desirable trait for electrocatalysis (Mannix et al., 2018) - though it is a metastable polymorph but can be stabilized via intercalation, electron beam irradiation and chemical exfoliation (Zhao et al., 2021). Despite the many interesting properties of TMDs, one major challenge that limits their widespread application in electrocatalysis is that their catalytic performance generally remains inferior to that of the PGM group. This limitation is primarily attributed to the chemical inertness of their basal planes, which constitute the majority of the exposed surface, while only edge sites contribute significantly to HER activity (Jaramillo et al., 2007). This severely limits their overall catalytic performance and practical utility. However, to activate the inert basal plane, defect engineering has emerged as a powerful and precise strategy for tailoring the surface chemistry and electronic properties of the 2D materials (Yin et al., 2016). The

**Correspondence:** Shamsuddeen Sani Alhassan. Department of Physics, Umaru Musa Yar'adua University, P.M.B. 2218, Katsina State, Nigeria. ✉ shamsuddeen.sani@umyu.edu.ng.

**How to cite**: Alhassan, S. S., Abdulsalam, M., Tanimu, A., & Bagudo, I. M. (2026). Chalcogen Vacancy Engineering in 1T-$TiS_2$, 1T-$TiSe_2$ and 1T-$TiTe_2$ Monolayers for Enhanced HER Activity: A DFT Study. *UMYU Scientifica*, 5(2), 312 – 322. https://doi.org/10.56919/usci.2652.029

intentional creation of chalcogen vacancies, in particular, can introduce localized states, modulate charge distribution, and create unsaturated metal sites, thereby optimizing the adsorption strength of reaction intermediates (Wang et al., 2013).

In this context, previous theoretical and experimental works have demonstrated that chalcogen vacancies can significantly enhance HER activity in the widely studied TMD-based electrocatalysts (the molybdenum (Mo)- and tungsten (W)-based TMDs) by shifting their Gibbs free energy of hydrogen adsorption ($\Delta G_{H^*}$) toward thermoneutral values, reducing the overpotentials, and increasing the number of active sites (Geng et al., 2020; Qing et al., 2019; Huang et al., 2022; Ogunkunle et al., 2024). However, titanium dichalcogenides ($TiX_2$; X = S, Se, Te), which are particularly attractive due to their low raw-material cost, earth abundance, corrosion resistance, and excellent chemical stability (Seh et al., 2017), have received relatively less attention (among the TMDs) in the area of electrocatalytic water splitting. Although the family members were extensively explored for other applications, such as in high-performance energy storage systems. $TiS_2$, the lightest among them, has garnered much attention in this regard due to its highest adsorption energy (Wu et al., 2021). A recent DFT study has shown that $TiS_2$ decorated with alkali metals (Li, Na, and K) could be a promising candidate for hydrogen storage applications (Iqrar et al., 2025). Other members ($TiSe_2$ and $TiTe_2$), though less studied, were reported to have exhibited some intriguing characteristics such as metallic property (for 1T phases), charge density wave (CDW), and superconductivity, which could be of great importance in the catalytic applications (Guesmi et al., 2023; Chen et al., 2017).

Among the very scarce studies reported on the catalytic capability of the family in HER is the work of Das and his co-researchers, who have shown that a single sulfur vacancy in a T-$TiS_2$ monolayer results in an appreciable $\Delta G_{H^*}$ value very close to zero (Das et al., 2019), which translates to a very good catalytic performance. Another DFT and machine learning study conducted by Ran et al. (2021) has also revealed that chalcogen vacancies in $TiSe_2$ and $TiTe_2$ have substantially decreased the $\Delta G_{H^*}$ values of the pristine systems, thereby improving their catalytic performance (Ran et al., 2021). In addition, experimental and theoretical investigations have confirmed that abundant sulfur vacancies in the $TiS_2$-x/NiS heterocatalyst effectively tune the electronic structures of metallic Ti and Ni atoms, thereby enhancing their HER catalytic kinetics (Wu et al., 2022). However, while Das et al. (Das et al., 2019) demonstrated near-zero $\Delta G_{H^*}$ for a single S-vacancy in $TiS_2$, their study was limited to $TiS_2$ and did not extend to the heavier chalcogenides (Se, Te) or provide a systematic comparison. Similarly, the machine-learning screening by Ran et al. (2021) identified promising candidates but did not provide a detailed mechanistic analysis of the electronic origins of HER enhancement or a controlled comparative DFT study under identical conditions across the entire 1T-$TiX_2$ family. To the best of our knowledge, no other studies have yet addressed this gap.

Therefore, motivated by this, in this work, we employ density functional theory (DFT) calculations to comprehensively and comparatively investigate how single X-vacancy engineering regulates the HER performance of the entire 1T-$TiX_2$ family. The single chalcogen vacancies are selected as the primary defect type because they represent the most thermodynamically accessible and experimentally most commonly observed point defect in TMDs (Kazemi et al., 2023; Zhou et al., 2013), and higher-order vacancy clusters may introduce structural complexity and strong geometric distortions that would obscure the fundamental electronic effects we seek to isolate. We systematically analyze the structural stability of defective structures (by computing their defect formation energies), hydrogen adsorption thermodynamics, electronic density of states, projected density of states, and charge density differences for both pristine and defective systems. Our results explain a clear structure-activity relationship, demonstrating that vacancy creation is a universal strategy for activating 1T-$TiX_2$ basal planes. This study provides fundamental insights and design principles for developing high-performance, vacancy-engineered TMD electrocatalysts for sustainable hydrogen generation.

## MATERIALS AND METHOD

### Computational Details

All calculations were performed based on first-principles approach within the framework of density functional theory (DFT), as implemented in the Quantum ESPRESSO code (Giannozzi et al., 2009). We used 2×2×1 supercells of 1T-$TiX_2$ (X = S, Se, Te) monolayers. The exchange-correlation functional was approximated using the generalized gradient approximation (GGA) with the Perdew-Burke-Ernzerhof (PBE) parameterization (Perdew et al., 1996). A plane-wave kinetic energy cutoff of 550 eV was applied. Convergence with respect to both the energy cutoff and the k-point density was verified (Figure 1): total energies were converged to within 1 meV/atom with respect to the cutoff. Electron-ion core interactions were treated using ultrasoft pseudopotentials for the valence orbitals of Ti ($4s^2\ 3d^2$), S ($3s^2\ 3p^4$), Se ($4s^2\ 4p^4$), Te ($5s^2\ 5p^4$), and H ($1s^1$)- the ultrasoft pseudopotentials (USPPs) were downloaded from the Quantum ESPRESSO pseudopotential library (PSlibrary). Brillouin zone integration was performed using an 8×8×1 Monkhorst-Pack k-point mesh (Monkhorst and Pack, 1976). A vacuum region of 20 Å was introduced in the z-direction to prevent spurious interactions between periodic images. Van der Waals interactions, which are significant for this class of materials, were incorporated using the DFT-D3 method (Alhassan et al., 2025; Grimme et al., 2010). Structures were fully relaxed using the BFGS algorithm until forces were less than 0.001 eV/Å. The electronic densities of states were calculated using a denser 16×16×1 k-point mesh. We note that the present calculations do not include explicit solvent, electrode potential, or pH corrections; these represent limitations that should be considered when comparing the computed thermodynamics to experimental HER measurements. A

sample of the QE input and output files (used in the study) is available in the supplementary file.

In acidic electrolytes, the HER proceeds via two primary mechanisms: Volmer–Tafel (equations 1 and 2) or Volmer–Heyrovsky (equation 3). The hydrogen adsorption site is indicated by the symbol "*" in this description (Fu et al., 2020).

$$* + H^+ + e^- \rightarrow H^*_{ads} \quad (1)$$

$$2H^*_{ads} \rightarrow H_2 + 2^* \quad (2)$$

$$* + H^+ + e^- + H^*_{ads} \rightarrow H_2 + * \quad (3)$$

The hydrogen adsorption step is common to both mechanisms and is very essential. However, the strength of this adsorption is quantified by the Gibbs free energy change (ΔGH*), a key descriptor of HER activity, and is calculated as (Huang et al., 2022; Ogunkunle et al., 2024).

$$\Delta G_{H^*} = \Delta E_{H^*} - T\Delta S + \Delta E_{ZPE}. \quad (4)$$

$$\Delta E_{H^*} = E_{H^*} - E_* - \frac{1}{2}E_{H_2}. \quad (5)$$

Where, $E_{H^*}$ and $E_*$ are the energies of the $TiX_2$ (X= S, Se, Te) monolayers with and without adsorbed H atoms, respectively, $E_{H_2}$ is the energy of the free $H_2$ molecule, T is the room temperature (T=300 K), ΔS is the entropy change, and $\Delta E_{ZPE}$ is the zero-point energy change. However, equation (4) can be written as (Norskov et al., 2005):

$$\Delta G_{H^*} = \Delta E_{H^*} + 0.24. \quad (6)$$

The theoretical overpotential $(\eta)$ is calculated in terms of $\Delta G_{H^*}$ according to the following equation (Ran et al., 2021):

$$\eta = \frac{-|\Delta G_{H^*}|}{e}. \quad (7)$$

However, to assess the stability of the defective structures, a defect formation energy ($E_f$) was calculated using the following equation (Huang et al., 2022):

$$E_f = E_D - E_P + \Delta n_i \sum_i \mu_i. \quad (8)$$

where, $E_D$ and $E_p$ are the total energies of the defective and pristine systems, $\Delta n_i$ is the difference in several atoms of type $i$ between those without and with the defect structure and $\mu_i$ is the corresponding chemical potential, referenced here to the elemental phases of the respective chalcogens.

## RESULTS AND DISCUSSION

### Convergence Tests with Respect to Kinetic Energy Cut-Off and K-Point Grids

To ensure the accuracy and numerical reliability of the DFT calculations, systematic convergence tests were conducted for the pristine 1T-$TiX_2$ (X = S, Se, and Te) monolayers. The total energy convergence was examined as a function of the plane-wave kinetic energy cutoff and k-point sampling density, with the results shown in Figures 1(a) and 1(b). The kinetic energy cutoff was varied between 10 and 55 Ry (136–748 eV), while the Monkhorst-Pack k-point grid was increased from 1 × 1 × 1 to 10 × 10 × 1. For all three systems, the total energy exhibited negligible variation beyond a cutoff energy of 40.45 Ry (550 eV) and an 8 × 8 × 1 k-point mesh. These parameters yielded an energy convergence better than 1 meV atom$^{-1}$ and were therefore adopted in all subsequent structural, electronic, and catalytic-property calculations.

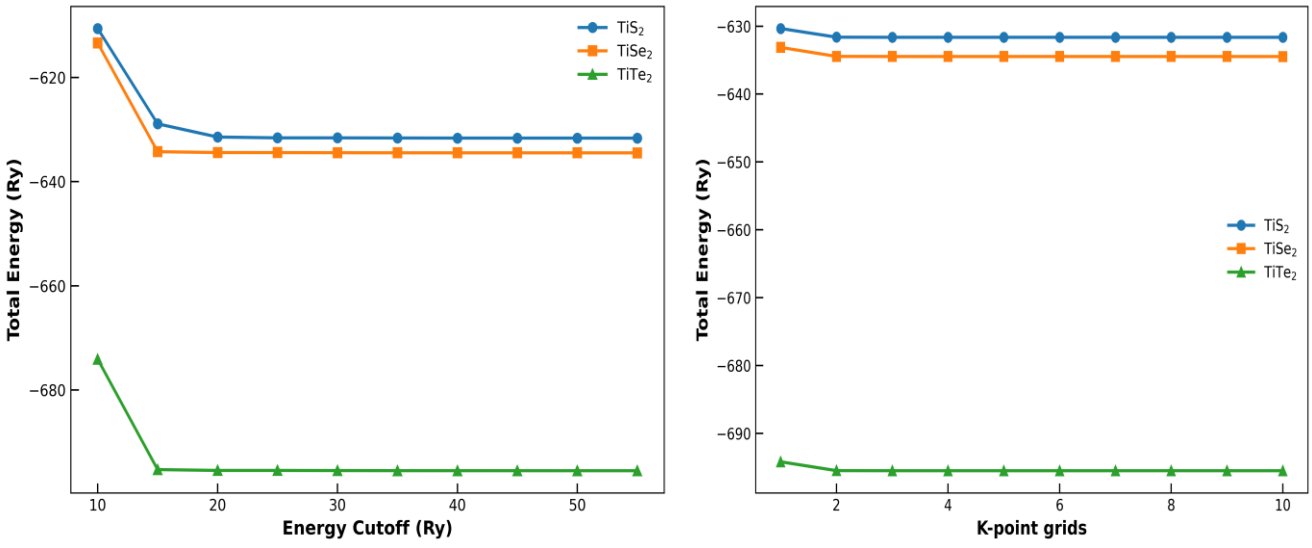


(a) (b)

**Figure 1: Convergence test calculation results with respect to: (a) kinetic energy cut-off (b) k-point sampling of the 1T-$TiX_2$(X=S, Se, Te) monolayers.**

### Structural Properties and Stability

The 1T-$TiX_2$ (X = S, Se, Te) phases crystallize into a trigonal $CdI_2$ structure with a space group of $P\bar{3}m1$(Zhao et al., 2021). The structures are made up of $TiX_6$ octahedral that share edges by connecting X atoms and Ti atoms located at the center of the octahedral coordination unit, as depicted in Figures 2(d) and 2(e). The optimized lattice constant (*a*) for the pristine 1T-$TiX_2$ (X= S, Se, Te) monolayers was calculated and listed in Table 1. The values are in good agreement with previous theoretical and experimental data (Das et al., 2019; Buslaps et al., 1993; Zhao et al., 2022; Zeng et al., 2011; Chen et al., 2017; Paliwal et al., 2024), validating our computational approach. However, the systematic increase in lattice constant seen from $TiS_2$ to $TiTe_2$ can be attributed to the increasing atomic radii of the chalcogen atoms (S < Se < Te), which leads to an expansion of the crystal lattice. However, this trend is consistent with the corresponding increase in titanium-chalcogen (Ti–X) bond lengths (Table 1), indicating weaker bonding interactions for heavier chalcogens. Additionally, the calculated adsorbed hydrogen-chalcogen (H–X) bond distances (Table 1) increase from H–S to H–Te, reflecting the increase in atomic radius as well as the electronegativity of the chalcogen atoms. This suggests a decreasing adsorption strength along S → Se → Te.

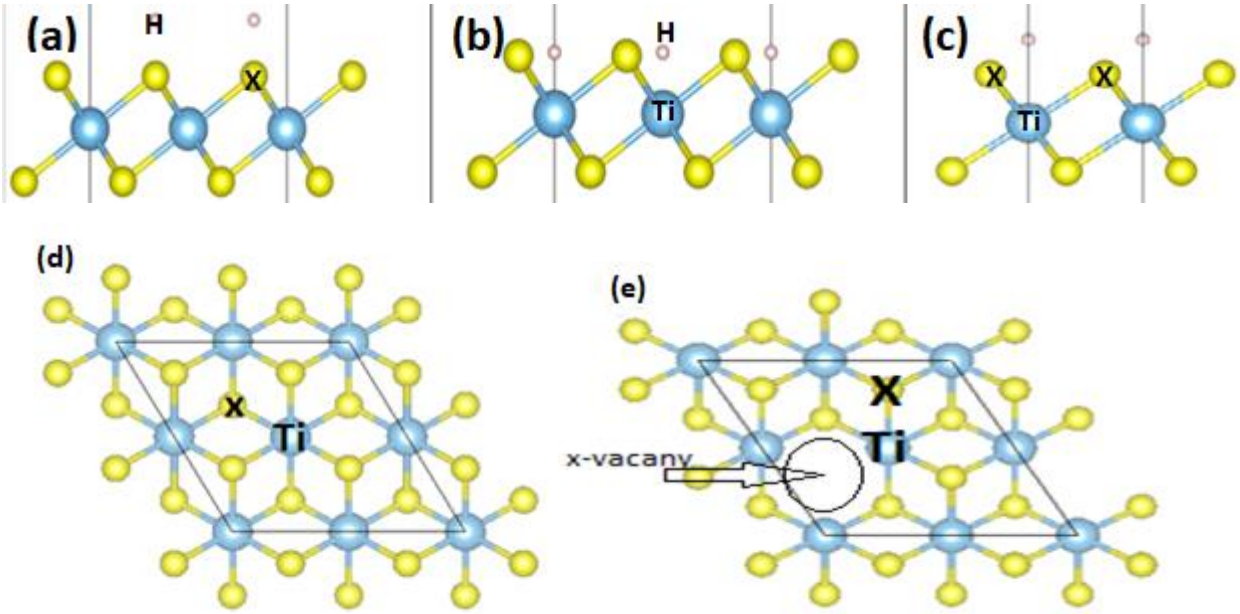


**Figure 2: H adsorption configurations at: (a) the X (X=S, Se, Te) (b) the Ti (c) bridge sites and optimized crystal structures of the: (d) pristine $TiX_2$(X=S, Se, Te) (e) defective $TiX_2$ monolayers showing the $TiX_6$ octahedral coordination.**

**Table 1: Calculated lattice parameter (*a*), titanium-chalcogen distance ($d_{Ti-X}$), adsorbed hydrogen-chalcogen distance ($d_{H-X}$), titanium-adsorbed hydrogen distance ($d_{Ti-H}$) and defect formation energies ($E_f$) for the 1T-$TiX_2$ (X=S, Se,Te) materials.**

| Material | *a*(Å) | | | $d_{Ti-X}$ (Å) | $d_{H-X}$ (Å) | $d_{Ti-H}$ (Å) | $E_f$ (eV) |
|---|---|---|---|---|---|---|---|
| | This work | Experimental | Theoretical | | | | |
| $TiS_2$ | 3.32 | 3.40 (Zeng et al., 2011) | 3.38 (Das et al., 2019) | 2.41 | 1.36 | 1.92 | 3.53 |
| $TiSe_2$ | 3.50 | 3.54 (Buslaps et al., 1993;Zhao et al., 2022) | 3.55 (Paliwal et al., 2024) | 2.53 | 1.54 | 1.76 | 2.73 |
| $TiTe_2$ | 3.66 | 3.78 (Chen et al., 2017) | 3.76 (Chen et al., 2017) | 2.77 | 1.69 | 1.82 | 2.12 |

However, a chalcogen (X) defect is employed in this work because it is easier to form (Kazemi et al., 2023). We also considered the most stable single chalcogen vacancy configuration. The calculated defect formation energies ($E_f$) are positive for all systems (Table 1), indicating that vacancies are thermodynamically stable and likely experimentally synthesizable. The $E_f$ values follow the order $TiS_2$ > $TiSe_2$ > $TiTe_2$, suggesting that Te vacancies form most easily, while S vacancies are the most difficult to create. This trend correlates with the decreasing strength of the Ti–X bond down the chalcogen group.

### Hydrogen Adsorption and Catalytic Activity

As adsorption energy is position-dependent (Pan et al., 2007), three different sites for hydrogen adsorption on the surface of 1T-$TiX_2$ (X = S, Se, Te) catalysts were considered, as depicted in Figures 2a, 2b, and 2c. They are on top of (i) Ti, (ii) X, and (iii) the bridge. The most stable and favourable adsorption sites for H were determined by calculating the adsorption energies at the three distinct positions using equation (5), and the results are shown in Figure 3. However, the results indicated that, for 1T-$TiS_2$ and 1T-$TiSe_2$ systems, the most stable adsorption site is on top of X (S or Se), in agreement with many previous

works (Das et al., 2019; Huang et al., 2022; Ogunkunle et al., 2024). In contrast to 1T-$TiTe_2$ material, where adsorption on top of Ti is found to be the most preferred and stable due to its lowest adsorption energy.

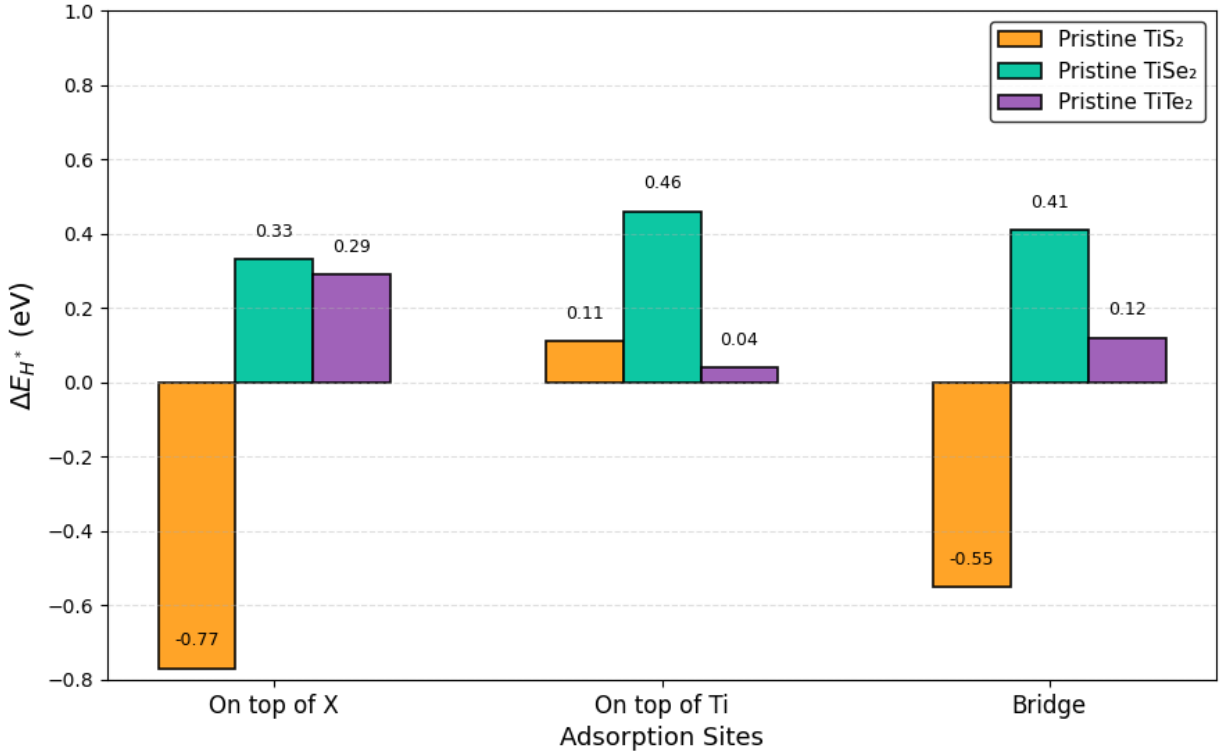


**Figure 3: Calculated adsorption energies for the three different sites on the surface of 1T-$TiX_2$ (X=S, Se, Te) monolayers.**

**Table 2: Calculated Gibbs free energy of hydrogen adsorption ($\Delta G_{H^*}$) and theoretical overpotential ($\eta$).**

| Materials | $\Delta G_{H^*}$ (eV) | $\eta$ (V) |
|---|---|---|
| Pure $TiS_2$ | -0.53 | -0.53 |
| Defective $TiS_2$ | -0.08 | -0.08 |
| Pure $TiSe_2$ | 0.57 | -0.57 |
| Defective $TiSe_2$ | -0.58 | -0.58 |
| Pure $TiTe_2$ | 0.28 | -0.28 |
| Defective $TiTe_2$ | 0.21 | -0.21 |

The catalytic activity of both pristine and defective1T-$TiX_2$ (S, Se, Te) monolayers toward HER is quantitatively evaluated using the Gibbs free energy change of hydrogen adsorption ($\Delta G_{H^*}$). The $\Delta G_{H^*}$ values for the most stable and favourable adsorption sites were calculated using equation (6), and the results are depicted in Figure 4a and Table 2. However, according to the established Sabatier principle, optimal catalytic performance is achieved when $\Delta G_{H^*}$ approaches zero, ensuring a balance between hydrogen adsorption and desorption (Fu et al., 2020; Norskov et al., 2005). Our result revealed that defective 1T-$TiS_2$ is closer to zero, with pristine 1T-$TiSe_2$ being the most distant from the optimal value (Figure 4a).

To gain a clearer understanding of the catalytic performance of the materials, a graph of theoretical overpotential versus ΔGH* (popularly known as a the volcano curve) is constructed for the pristine and defective 1T-$TiX_2$ (X = S, Se, Te) monolayers and presented in Figure 4b. Pt(111) is always used as a benchmark HER catalyst, as it appears near the apex of the volcano ($\Delta G_{H^*} \approx -0.09$ eV), confirming its superior HER activity (Man et al., 2011; Xu et al., 2018).

Figure 4b shows that the pristine 1T-$TiX_2$ (X = S, Se, Te) systems deviate significantly from the volcano peak. Pristine $TiS_2$ lies on the strong hydrogen-binding side (left), indicating excessive adsorption that impedes $H_2$ desorption, whereas pristine 1T-$TiSe_2$ and 1T-$TiTe_2$ fall on the weak-binding side (right), where insufficient hydrogen adsorption occurs, leading to sluggish Volmer kinetics. These unfavorable adsorption characteristics explain their comparatively poor intrinsic HER activity. Moreover, the introduction of X vacancies leads to a pronounced shift of all 1T-$TiX_2$ systems toward the volcano apex. In particular, defective 1T-$TiS_2$ exhibits a $\Delta G_{H^*}$ value close to zero, comparable to that of Pt (111), indicating optimal hydrogen binding. This near-thermoneutral hydrogen adsorption suggests optimal catalytic behaviour, with minimal kinetic barriers for both adsorption and desorption. Defective 1T-$TiSe_2$ and 1T-$TiTe_2$ also show significant improvements relative to their

pristine counterparts, although their $\Delta G_{H^*}$ values remain moderately displaced from the optimal region. This indicates that while vacancy-induced electronic modulation significantly enhances HER activity across the 1T-$TiX_2$ family, the degree of enhancement is strongly chalcogen-dependent.

The volcano plot therefore, establishes a clear activity trend: defective $TiS_2$ > defective $TiTe_2$ > defective $TiSe_2$, and confirms defective 1T-$TiS_2$ as the most promising non-precious HER catalyst among the studied systems. The fact that the defective 1T-$TiS_2$ achieves a $\Delta G_{H^*}$ (-0.08 eV), which is within 0.01 eV of the Pt (111) benchmark (-0.09 eV) on a purely thermodynamic basis does not confirm equivalent catalytic performance, further descriptors need to be investigated, such as exchange current density, turnover frequency, kinetic barriers, and electrode/solvent effects, as the HER is pH-dependent.

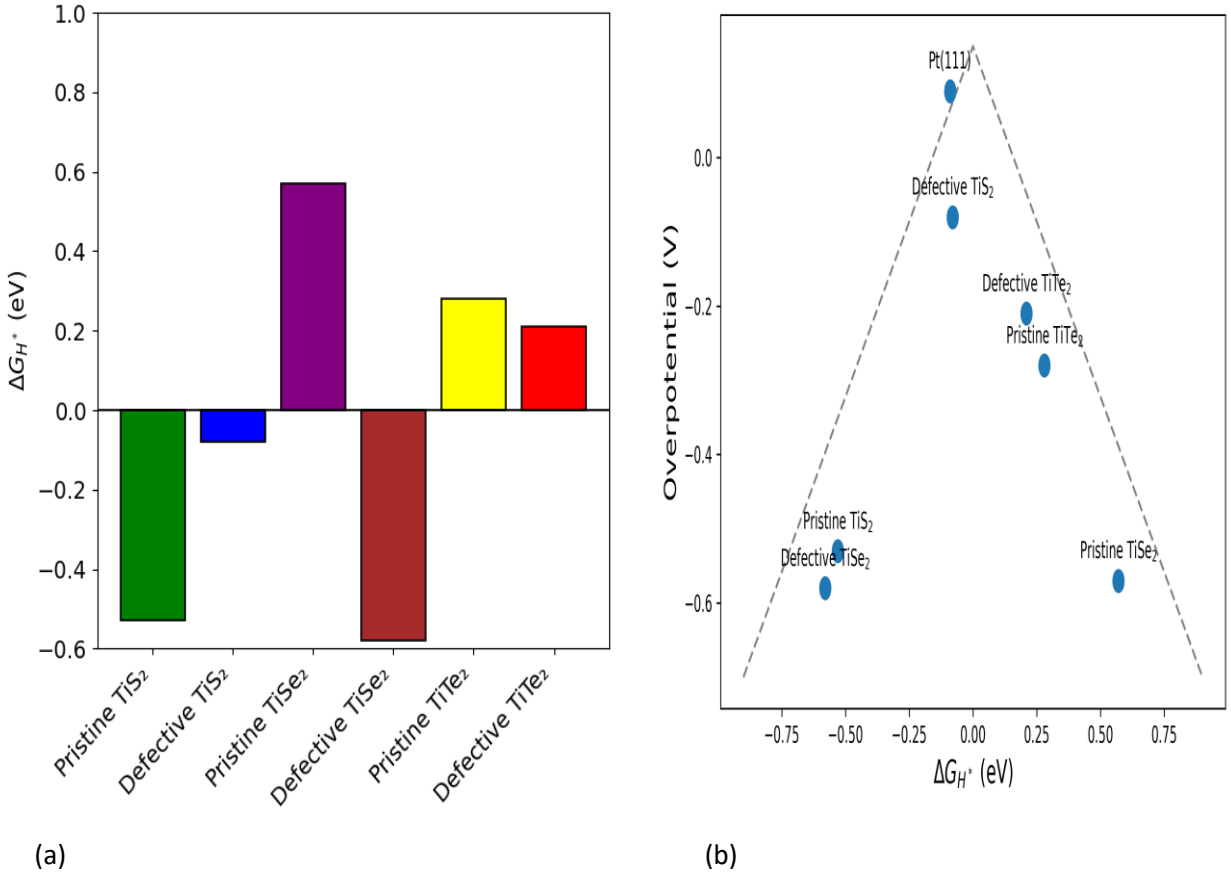


**Figure 4: (a) Calculated values of ($\Delta G_{H^*}$) (b) Volcano plot constructed using the Gibbs free energy of hydrogen adsorption ($\Delta G_{H^*}$) and theoretical overpotential for pristine and defective 1T-$TiX_2$ (X = S, Se, Te) monolayers, with Pt (111) included as a reference catalyst.**

**Density of States (DOS) and Projected Density of States (PDOS)**

To further explain the electronic origins of the observed enhancement in HER activity, the electronic density of states (DOS) and projected density of states (PDOS) of both pristine and defective 1T-$TiX_2$ (X= S, Se, Te) systems are analyzed, as shown in Figure 5. The DOS plots always reveal the number of available electronic states at different energy levels. However, the electronic states near the Fermi level plays a crucial role in governing charge-transfer kinetics and catalytic efficiency (Deng et al., 2019; Vojvodic et al., 2014).

Pristine 1T-$TiS_2$ (Figure 5a) exhibits semi-metallic behavior, characterized by a very low density of states at the Fermi level (Tanwar et al., 2023; Guesmi et al., 2023). This limited availability of electronic states near $E_f$ impedes efficient electron transfer during HER, contributing to its suboptimal catalytic performance despite strong hydrogen adsorption. In contrast, pristine 1T-$TiSe_2$ (Figure 5c) and 1T-$TiTe_2$ (Figure 5e) display metallic characteristics, with finite DOS at the Fermi level, consistent with a previous report (Guesmi et al., 2023). However, metallicity alone is insufficient to guarantee high HER activity, as reflected by their unfavorable hydrogen adsorption energetics. It is clearly seen that the valence bands of the three pristine systems are dominated by hybridised Ti-d and X (X=S, Se, Te) p orbitals, while the conduction bands are are largely populated by the Ti-d orbital.

In addition, the introduction of X vacancies induces pronounced modifications in the electronic structure of all $TiX_2$ (X= S, Se, Te) systems. In defective 1T-$TiS_2$ (Figure 5b) sulfur vacancies generate prominent electronic states crossing the Fermi level, driving a transition from semi-

metallic to metallic behavior. This vacancy-induced metallization significantly enhances electronic conductivity and facilitates rapid electron transfer to adsorbed hydrogen intermediates, thereby explaining the superior HER activity of defective $TiS_2$ (Wang et al., 2019).

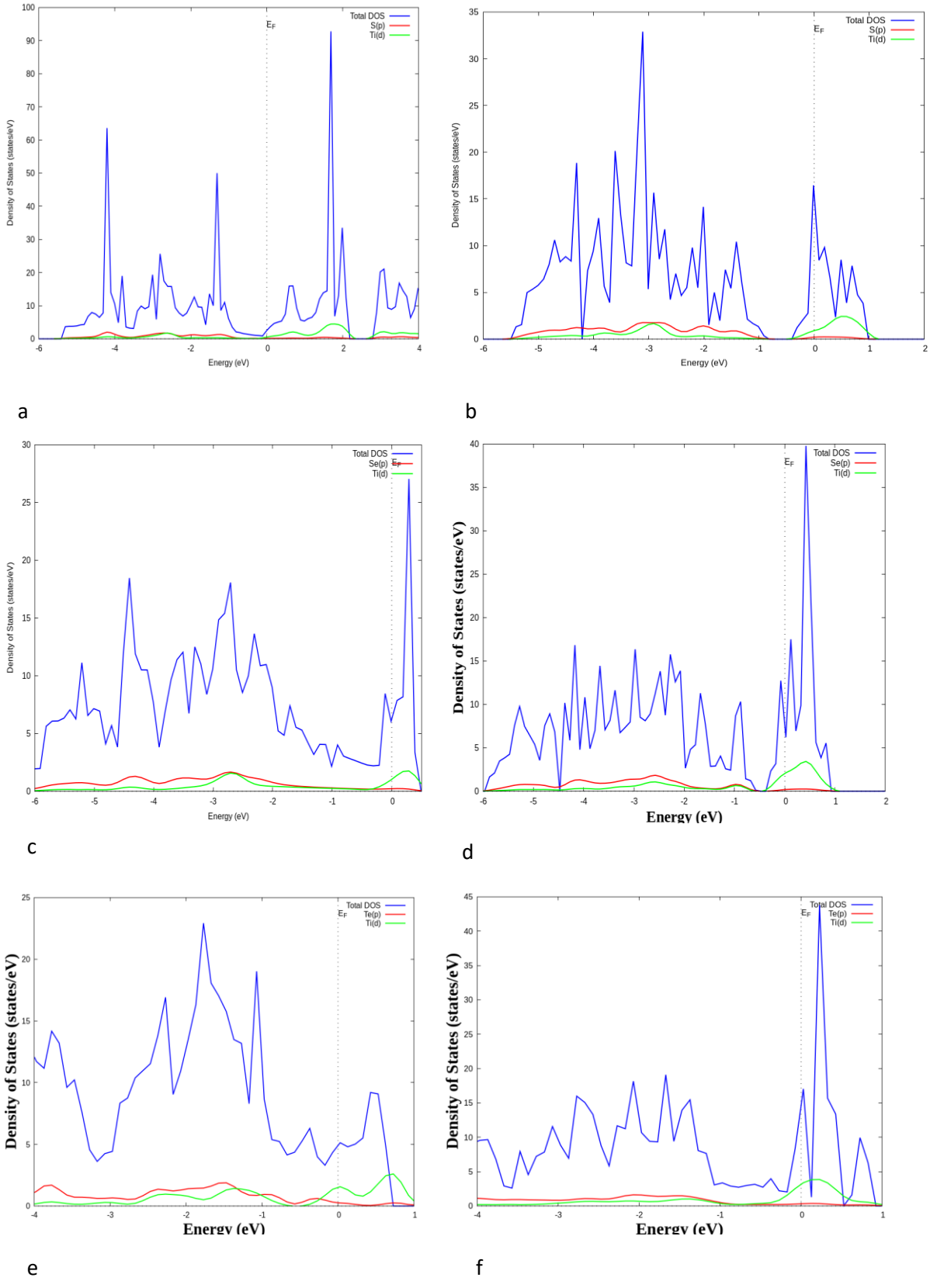


**Figure 5: TDOS/PDOS plots for the (a) Pristine $TiS_2$ (b) Defective $TiS_2$ (c) Pristine $TiSe_2$ (d) Defective $TiSe_2$ (e) Pristine $TiTe_2$ (f) Defective $TiTe_2$. The Fermi level is set to 0.0 eV.**

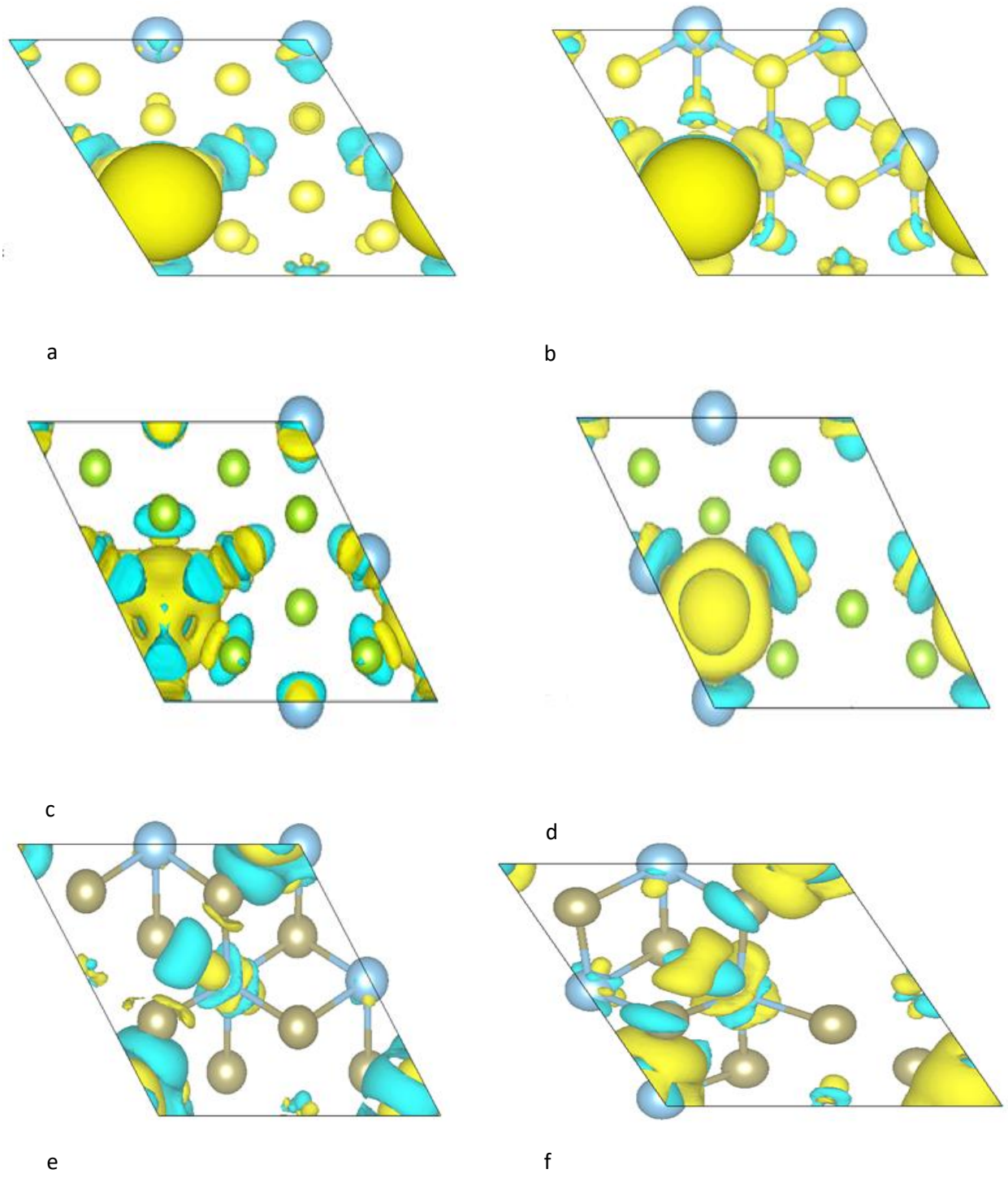


**Figure 6: Charge density difference (CDD) isosurfaces (±0.0014 e Å⁻³) for hydrogen adsorption on: (a) pristine $TiS_2$ (b) defective $TiS_2$ (c) pristine $TiSe_2$ (d) defective $TiSe_2$ (e) pristine $TiTe_2$ and (f) defective $TiTe_2$. Yellow regions indicate electron accumulation; cyan regions indicate electron depletion.**

Similarly, selenium and tellurium vacancies in $TiSe_2$ (Figure 5d) and $TiTe_2$ (Figure 5f) introduce additional states near the Fermi level, primarily arising from unsaturated Ti d-orbitals. These states enhance charge density at the active sites and strengthen catalyst–adsorbate interactions, thereby improving HER performance relative to pristine systems. Nevertheless, the electronic enhancement is less pronounced, than in defective $TiS_2$, consistent with their comparatively inferior catalytic activity observed in the volcano analysis.

**Charge Density Difference (CDD) Analysis**

Charge density difference (CDD) analysis was performed to visualise and quantify the spatial redistribution of electronic charge upon hydrogen adsorption on both pristine and defective $TiX_2$ (X = S, Se, Te) surfaces. The CDD is defined as (Huang et al., 2022):

$$\Delta\rho = \rho_{(catalyst+H)} - \rho_{(catalyst)} - \rho_{(H)} \quad (9)$$

where $\rho_{(catalyst+H)}$, $\rho_{(catalyst)}$, and $\rho_{(H)}$ are the charge densities of the $TiX_2$ monolayer with adsorbed H, without adsorbed H and the isolated H atom, respectively. Regions of charge accumulation ($\Delta\varrho > 0$) and charge depletion ($\Delta\varrho < 0$) are depicted in yellow and cyan isosurfaces (isosurface value: $\pm 0.0014$ e Å$^{-3}$) in Figure 6.

For the pristine $TiS_2$, $TiSe_2$ and $TiTe_2$ systems (Figures 6a, 6c and 6e), charge redistribution is more localised around the adsorption site, suggesting the possibility of a moderate interaction between adsorbed hydrogen and the catalyst surface. The charge accumulation observed around the adsorbed H atom for all the materials demonstrates a charge transfer from the pristine TiX2 to the adsorbate (H), similar to what has been reported in the literature for a related 2D material (Huang et al., 2022).

The defective systems (Figures 6b, 6d, and 6f) exhibit stronger charge accumulation around the adsorption regions than the pristine materials. This increased charge redistribution is a clear indication of improved electron transfer and a stronger interaction between the adsorbed hydrogen and the $TiX_2$ surface. However, this suggests enhanced electrical conductivity and optimized adsorption behavior, both of which are essential for efficient hydrogen evolution reaction (HER) activity.

## CONCLUSION

This research provides a systematic, mechanistic understanding of how X vacancies regulate the HER activity of 1T-$TiX_2$ (X = S, Se, Te) monolayers. First-principles calculations confirm that pristine $TiX_2$ surfaces suffer from intrinsically unbalanced hydrogen adsorption, which limits their catalytic efficiency. By contrast, the intentional creation of X vacancies induces profound modifications in both surface chemistry and electronic structure, driving the $\Delta G_{H^*}$ toward thermoneutral values and significantly enhancing catalytic performance.

Among the studied systems, defective 1T-$TiS_2$ emerges as the most active HER catalyst, with a $\Delta GH^*$ value that closely matches that of the optimal Pt (111) reference. Volcano plot analysis unequivocally demonstrates that vacancy engineering shifts $TiX_2$ monolayers toward the activity maximum, while DOS and PDOS calculations reveal vacancy-induced metallic states near the Fermi level that promote efficient electron transfer during HER. Charge density difference analysis further indicates stronger charge accumulation around the adsorbed H atom in the defective systems. In addition, the calculated defect formation energy values indicate that these defective structures are thermodynamically stable and may be experimentally feasible.

In conclusion, this DFT study identifies chalcogen vacancy engineering as a computationally promising strategy for activating the basal planes of 1T-$TiX_2$ monolayers toward HER. Among the studied systems, defective $TiS_2$ emerges as the most computationally promising candidate, with near-thermoneutral hydrogen adsorption, positioning it as a strong lead for experimental investigation. However, realizing these computational predictions as practical, high-performance electrocatalysts will require experimental validation, stability testing under HER operating conditions, and further theoretical investigation of kinetic barriers, solvent/electrode effects, and long-term stability. This work therefore provides design principles and a theoretical foundation - rather than a confirmed replacement - for guiding the rational development of next-generation, vacancy-engineered $TiX_2$-based HER electrocatalysts

## DATA AVAILABILITY

The data used in the study will be made available from the corresponding author upon request.

## ACKNOWLEDGMENT

The authors gratefully acknowledge the financial support of Umaru Musa Yar'adua University, Katsina, under the staff training and development (STD) scheme.

## REFERENCES

Alhassan, S. S., Abdulsalam, M., & Tanimu, A. (2025). Application of transition metals dichalcogenides in electrocatalytic splitting of water for hydrogen production: A review. *Nigerian Journal of Physics*, 34, 44. [Crossref]

Alhassan, S. S., Abdulsalam, M., Tanimu, A., & Bagudo, I. M. (2025). Role of Van der Waals correction on the catalytic performance of 1T-$TiS_2$ electrocatalyst. *African Scientific Reports*, 4, 356. [Crossref]

Buslaps, T., Johnson, R. L., & Jungk, G. (1993). Spectroscopic ellipsometry on 1T-$TiSe_2$. *Thin Solid Films*, 234, 549-552. [Crossref]

Chen, P., Pai, W. W., Chan, Y.-H., Takayama, A., Xu, C.-Z., Chou, M. Y., Mo, S.-K., Fedorov, A.-V., & Chiang, T.-C. (2017). Emergence of charge density waves and a pseudogap in single-layer $TiTe_2$. *Nature Communications*, 8, 516. [Crossref]

Chhowalla, M., Liu, Z., & Zhang, H. (2015). Two-dimensional transition metal dichalcogenide (TMD) nanosheets. *Chemical Society Reviews*, 44, 2584-2606. [Crossref]

Das, T., Chakraborty, S., Ahuja, R., & Das, G. P. (2019). $TiS_2$ monolayer as an emerging ultrathin bifunctional catalyst: Influence of defects and functionalization. *ChemPhysChem*, 20, 608-615. [Crossref]

Deng, C., He, R., Shen, W., Li, M., & Zhang, T. (2019). A single-atom catalyst of cobalt supported on a defective two-dimensional boron nitride material as a promising electrocatalyst for the oxygen reduction reaction: A DFT study. *Physical Chemistry Chemical Physics*, 21, 6900-6907. [Crossref]

Fu, Q., et al. (2020). 2D transition metal dichalcogenides: Design, modulation, and challenges in electrocatalysis. *Advanced Materials*, 32, 1907818. [Crossref]

Geng, S., Yang, W., Liu, Y., & Yu, Y. (2020). Engineering sulfur vacancies in basal plane of $MoS_2$ for

enhanced hydrogen evolution reaction. *Journal of Catalysis*, 391, 91-97. [Crossref]

Giannozzi, P., et al. (2009). Quantum ESPRESSO: A modular and open-source software project for quantum simulations of materials. *Journal of Physics: Condensed Matter*, 21, 395502. [Crossref]

Grimme, S., Antony, J., Ehrlich, S., & Krieg, H. (2010). A consistent and accurate ab initio parametrization of density functional dispersion correction (DFT-D) for the 94 elements H-Pu. *Journal of Chemical Physics*, 132, 154104. [Crossref]

Guesmi, I., Bouammali, M. A., Malki, S., Darhi, Z., Challioui, A., & El Farh, L. (2023). Theoretical investigation of optoelectronics properties of titanium dichalcogenides materials $TiX_2$ (X = S, Se, Te) using Quantum ESPRESSO. *Materials Science Forum*, 1095, 21-35. [Crossref]

Huang, H., Hu, G., Hu, C., & Fan, X. (2022). Enhanced hydrogen evolution reactivity of T'-phase tungsten dichalcogenides ($WS_2$, $WSe_2$, and $WTe_2$) materials: A DFT study. *International Journal of Molecular Sciences*, 23, 11727. [Crossref]

Iqrar, U., Alarfaji, S. S., Nabi, G., & Khan, M. I. (2025). Light-metal decorated titanium disulfide as an efficient hydrogen storage material: A DFT study. *International Journal of Hydrogen Energy*, 169, 151115. [Crossref]

Jaramillo, T. F., Jørgensen, K. P., Bonde, J., Nielsen, J. H., Horch, S., & Chorkendorff, I. (2007). Identification of active edge sites for electrochemical $H_2$ evolution from $MoS_2$ nanocatalysts. *Science*, 317, 100-102. [Crossref]

Kazemi, S. A., Yengejeh, S. I., Ogunkunle, S. A., Wen, Z. L., Liew, A. W. C., & Wang, Y. (2023). Vacancy impacts on electronic and mechanical properties of $MX_2$ (M = Mo, W and X = S, Se) monolayers. *RSC Advances*, 13, 6498-6506. [Crossref]

Man, I. C., Su, H. Y., Calle-Vallejo, F., Hansen, H. A., Martinez, J. I., Inoglu, N. G., Kitchin, J., Jaramillo, T. F., Nørskov, J. K., & Rossmeisl, J. (2011). Universality in oxygen evolution electrocatalysis on oxide surfaces. *ChemCatChem*, 3, 1159-1165. [Crossref]

Mannix, A. J., Zhang, Z., Guisinger, N. P., Yakobson, B. I., & Hersam, M. C. (2018). Borophene as a prototype for synthetic 2D materials development. *Nature Nanotechnology*, 13, 444-450. [Crossref]

Monkhorst, H. J., & Pack, J. D. (1976). Special points for Brillouin-zone integrations. *Physical Review B*, 13, 5188-5192. [Crossref]

Nørskov, J. K., Bligaard, T., Logadottir, A., Kitchin, J., Chen, J. G., Pandelov, S., & Stimming, U. (2005). Trends in the exchange current for hydrogen evolution. *Journal of the Electrochemical Society*, 152, J23-J26. [Crossref]

Ogunkunle, S. A., Bouzid, A., Hinsch, J. J., Allen, O. J., White, J. J., Bernard, S., Wu, Z., Zhu, Y., & Wang, Y. (2024). Defect engineering of 1T' $MX_2$ (M = Mo, W and X = S, Se) transition metal dichalcogenide-based electrocatalyst for alkaline hydrogen evolution reaction. *Journal of Physics: Condensed Matter*, 36, 145002. [Crossref]

Pan, H., Feng, Y. P., & Lin, J. (2007). Hydrogen adsorption by tungsten carbide nanotube. *Applied Physics Letters*, 90, 223104. [Crossref]

Paliwal, U., Tanwar, P., & Joshi, K. B. (2024). Structural, electronic and thermoelectric properties of monolayer $TiSe_2$. *Journal of Molecular Modeling*, 30, 80. [Crossref]

Perdew, J. P., Burke, K., & Ernzerhof, M. (1996). Generalized gradient approximation made simple. *Physical Review Letters*, 77, 3865-3868. [Crossref]

Qing, Z., Wenzhou, C., Hua, C., Zhouguang, L., & Hui, P. (2019). $WS_2$ nanosheets with highly-enhanced electrochemical activity by facile control of sulfur vacancies. *ChemCatChem*, 11, 4219-4225. [Crossref]

Ran, N., Sun, B., Qiu, W., Song, E., Chen, T., & Liu, J. (2021). Identifying metallic transition-metal dichalcogenides for hydrogen evolution through multilevel high-throughput calculations and machine learning. *Journal of Physical Chemistry Letters*, 12, 2102-2111. [Crossref]

Seh, Z. W., Kibsgaard, J., Dickens, C. F., Chorkendorff, I., Nørskov, J. K., & Jaramillo, T. F. (2017). Combining theory and experiment in electrocatalysis: Insights into materials design. *Science*, 355, eaad4998. [Crossref]

Stamenkovic, V. R., Strmcnik, D., Lopes, P. P., & Markovic, N. M. (2017). Energy and fuels from electrochemical interfaces. *Nature Materials*, 16, 57-69. [Crossref]

Sukanya, R., da Silva Alves, D. C., & Breslin, C. B. (2022). Recent developments in the applications of 2D transition metal dichalcogenides as electrocatalysts in the generation of hydrogen for renewable energy conversion. *Journal of the Electrochemical Society*, 169, 064504. [Crossref]

Tanwar, P., Paliwal, U., Joshi, K. B., & Kumar, J. (2023). First-principles study of structural, electronic and vibrational properties of bulk and monolayer $TiS_2$. *Journal of Physics and Chemistry of Solids*, 179, 111382. [Crossref]

Vojvodic, A., Nørskov, J. K., & Abild-Pedersen, F. (2014). Electronic structure effects in transition metal surface chemistry. *Topics in Catalysis*, 57, 25-32. [Crossref]

Wang, H., et al. (2013). Electrochemical tuning of vertically aligned $MoS_2$ nanofilms and its application in improving hydrogen evolution reaction. *Proceedings of the National Academy of Sciences*, 110, 19701-19706. [Crossref]

Wang, J., Liu, Y.-P., Zhang, H., Huang, D.-J., & Chu, K. (2019). Ambient electrocatalytic nitrogen reduction on a $MoO_2$/graphene hybrid: Experimental and DFT studies. *Catalysis Science and Technology*, 9, 4248-4254. [Crossref]

Wu, J., Zhong, W., Yang, C., Xu, W., Zhao, R., Xiang, H., Zhang, Q., Li, X., & Yang, N. (2022). Sulfur-vacancy rich nonstoichiometric $TiS_2$-x/NiS

heterostructures for superior universal hydrogen evolution. *Applied Catalysis B: Environmental*, 310, 121332. [Crossref]

Wu, Q., Chen, Y., Hao, X., Zhu, T., Cao, Y., & Wang, W. (2021). Insight into the anchoring effect of two-dimensional $TiX_2$ (X = S, Se, Te) materials for lithium-sulfur batteries: A DFT study. *Journal of the Electrochemical Society*, 168, 120516. [Crossref]

Xu, H. X., Cheng, D. J., Cao, D. P., & Zeng, X. C. (2018). A universal principle for a rational design of single-atom electrocatalysts. *Nature Catalysis*, 1, 339-348. [Crossref]

Yin, Y., et al. (2016). Contributions of phase, sulfur vacancies, and edges to the hydrogen evolution reaction catalytic activity of porous molybdenum disulfide nanosheets. *Journal of the American Chemical Society*, 138, 7965-7972. [Crossref]

Zeng, Z., Yin, Z., Huang, X., Li, H., He, Q., Lu, G., Boey, F., & Zhang, H. (2011). Single-layer semiconducting nanosheets: High-yield preparation and device fabrication. *Angewandte Chemie International Edition*, 50, 11093-11097. [Crossref]

Zhao, B., Shen, D., Zhang, Z., Lu, P., Hossain, M., Li, J., Li, B., & Duan, X. (2021). 2D metallic transition-metal dichalcogenides: Structures, synthesis, properties, and applications. *Advanced Functional Materials*, 31, 2105132. [Crossref]

Zhao, W.-M., et al. (2022). Moiré enhanced charge density wave state in twisted 1T-$TiTe_2$/1T-$TiSe_2$ heterostructures. *Nature Materials*, 21, 284-290. [Crossref]

Zhou, W., Zou, X., Najmaei, S., Liu, Z., Shi, Y., Kong, J., Lou, J., Ajayan, P. M., Yakobson, B. I., & Idrobo, J.-C. (2013). *Nano Letters*, 13, 2615-2622. [Crossref]

Zhu, J., Hu, L., Zhao, P., Lee, L. Y. S., & Wong, K. Y. (2020). Recent advances in electrocatalytic hydrogen evolution using nanoparticles. *Chemical Reviews*, 120, 851-918. [Crossref]